



Sensitivity Improvement for PET System

Paul Glaysher, University of Bristol, UK

September 8, 2011

Abstract

Positron Emission Tomography is a powerful tool in nuclear medicine for the diagnosis and treatment of various diseases such as cancer, Huntingtons and Alzheimer's. The benefit of a PET scan must however be weighed against the potential health damage caused by the exposure to the injected radio-tracer. Therefore any improvement of the PET sensitivity, would decrease to dose on the patient of currently 10mSv and make this imaging technique more applicable. The sensitivity of a PET device is reduced by Compton scattering in the patient as well as in the scintillator crystals of the detector units. A method of recovering the loss due to the latter is presented in this report.

Contents

1	Introduction to PET	3
2	Imaging principle in PET	4
3	PET Prototype	4
3.1	Scintillator Crystal	5
3.2	SiPM	6
4	Gamma Ray Spectrum	7
5	Motivation - Sensitivity Losses in PET	9
6	Experimental Setup	10
7	Results	11
8	Discussion	13
8.1	Reconstruction Issue	13
8.2	Readout Issue	15
9	Conclusion	15
10	Acknowledgements	15

1 Introduction to PET

Positron Emission Tomography is a non invasive imaging technique used in nuclear medicine, for which radio-nuclide tracer substances are injected into the patient.

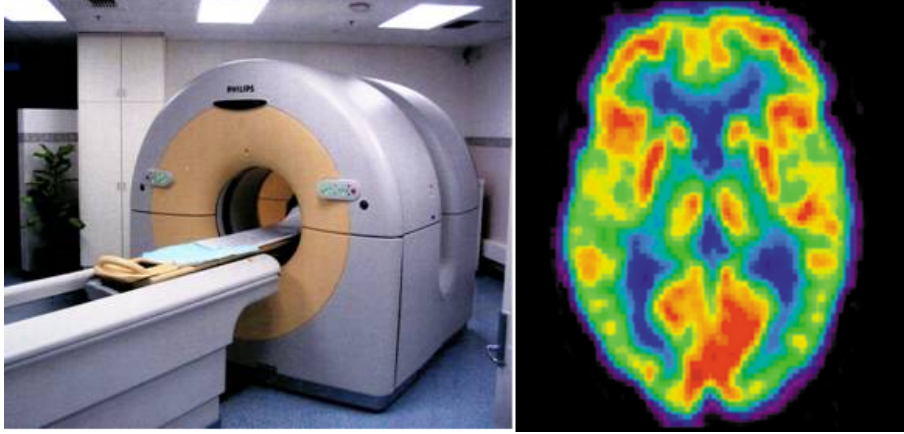


Figure 1: Example of a commercial PET device and a a PET scan of the brain.

Information on tissue metabolism and physiology can be gained from PET scans, unobtainable by Computed Tomography (CT) or Magnetic Resonance Imaging (MRI), as these only image the body's structure and anatomy. PET scanning traces the position and movement of any compound in any organ as long as it can be radio-labeled with a positron emitter. A typical PET and an image it produces is shown in Figure 1. Radio-nuclides commonly used in PET scanning consist of short lived isotopes, as listed in Figure 2, which are incorporated into biochemical compounds found in our body, such as glucose, receptors or water, providing labeled compounds that take part in metabolic and physiological processes. Consequently these processes themselves can be probed. For example, small animal PET is also used for monitoring drug trials on mice or rats. The synthesis of radio-nuclides for certain processes is a limiting factor in studying a metabolic or physiological process, especially as their production requires specialised cyclotron facilities.

Radionuclide	$\tau_{1/2}$ [min]	E_{max} [MeV]	R_{mean} [mm]	R_{max} [mm]
^{15}O	2.03	1.738	2.5	7.3
^{13}N	9.96	1.197	1.5	5.1
^{11}C	20.4	0.959	1.1	4.1
^{18}F	109.8	0.633	0.6	2.4

Figure 2: List of commonly used radio-nuclides in PET [5]

The most important radio-nuclide for cancer treatment is Fludeoxyglucose (FDG), with the same biological properties of glucose but labelled with fluorine-18. ^{18}F is chosen over other nuclides for its preferable properties with respect to its half-life $\tau_{1/2}$ and free-mean-path R_{mean} , as in Figure 2. A $\tau_{1/2}$ of 110min is sufficient to perform a scan with a high rate but does not dose the patient unnecessarily after the examination. A short R_{mean} of 0.6mm ensures a good spatial resolution of the PET device. When injected, FDG accumulates in tissue regions of high metabolic activity, such as tumour cells.

2 Imaging principle in PET

The positrons emitted from the source have a mean free path in the order of a few mm in water, the main component of our body, and annihilate with thermal electrons in the tissue. In this process two photons with an energy of 511keV each are produced, equivalent to the electron rest-mass, propagating nearly back to back, required by momentum conservation. A simultaneous detection of two 511keV gamma rays defines the line of their path, on which the location of the positron source lies. This construction is called line of response (LOR), presented in Figure 3. The intersections of multiple superimposed LOR produce a real time, two or three dimensional map of the positron emitter density in the patient.

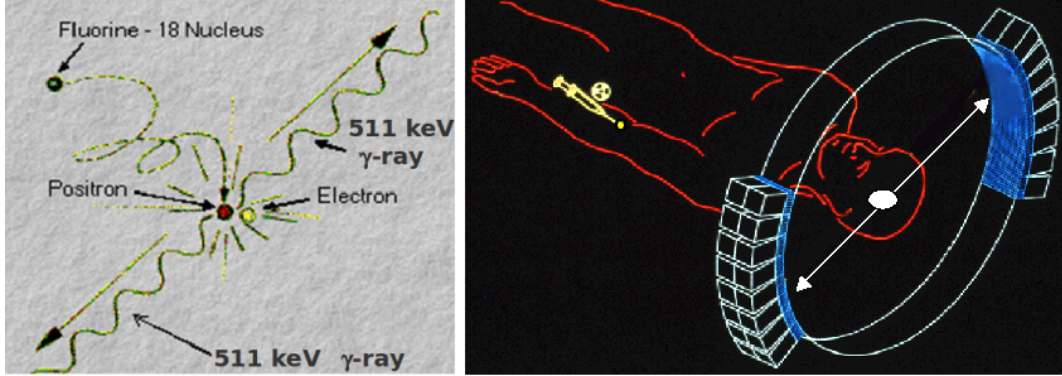


Figure 3: Detection of coincident gamma rays produces a line of response.

3 PET Prototype

The PET prototype is a 32 channel arrangement used for hardware investigations, but unsuited for medical imaging. Four side-by-side Silicon Photomultiplier (SiPM) chips directly mounted onto scintillator crystals make up a detector unit, the SiPMs in turn contain four channels per chip. The two detector units are fixed on a rotating table, allowing the investigation of various detector-source geometries.

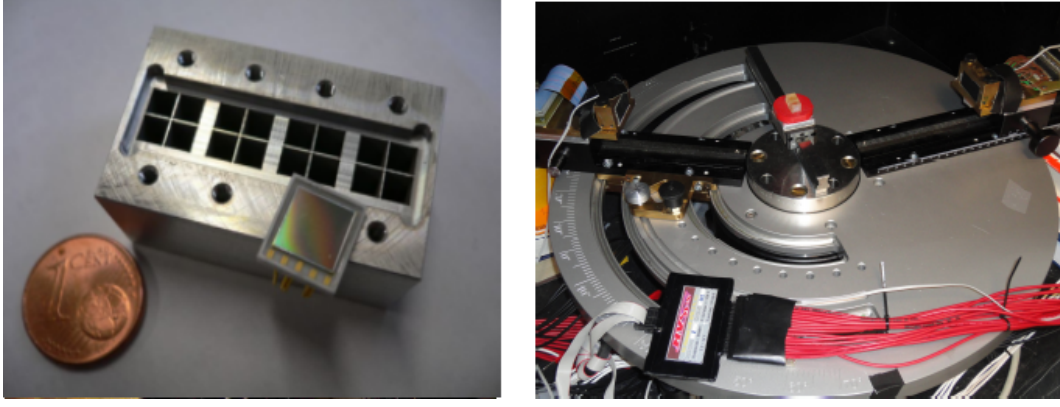


Figure 4: The SiPM chips are 6x6mm in size and the crystal are 6x6x15mm. Both detector units with a source place in the center.

The PET prototype has a spatial resolution of 2mm and is therefore capable of resolving objects with a minimum separation of 4mm, as demonstrated in Figure 5. From this plot the energy resolution can also be evaluated at 13%.

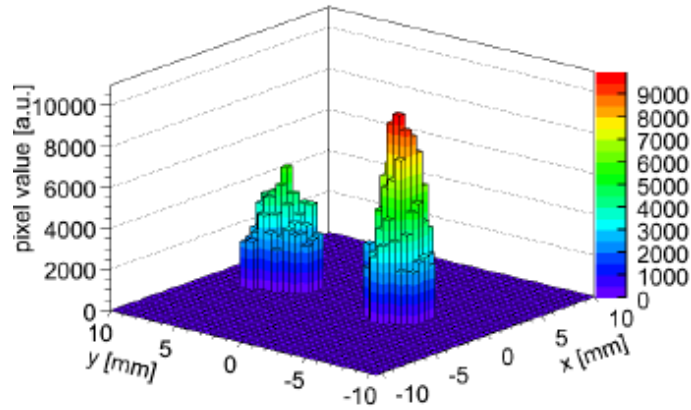


Figure 5: Example of 2 point-like sources 1cm apart.

The channels are individually powered at around 71V and connected to an ADC board.

3.1 Scintillator Crystal

A scintillator is a material with which particles or photons interact, depositing their energy, which in turn is converted into in the visible to UV range. The number of generated photons is directly proportional the energy deposited. The scintillator crystals used are made of Lutetium-Oxyorthosilicate (LSO), a high Z and high density (7.3 gcm^{-3}) material that can be cut into small sizes. This inorganic scintillator has its emission peak at 420nm and an intrinsic energy resolution of 9%. Consulting Table 1,

the choice of LSO for its short decay time for PET becomes obvious. A short decay time allows to distinguish between two independent events with a small time difference.

Crystal	Att. length at 511keV[mm]	Light yield	Emission peak [nm]	Decay time
BGO	10.4	15	480	300
NaI	28.6	100	410	230
GSO	14.1	30	440	60
LSO	11.4	75	420	40

Table 1: Comparison of alternatives to LSO [1].

3.2 SiPM

Capable of counting single photons, SiPMs are arrays of Avalanche Photo Diodes(APD) working in Geiger mode.

SiPMs have a comparable gain and time resolution to the traditionally used vacuum Photo Multiplier Tubes (PMT), presented in Table 3.2.

	SiPM	PMT
Gain	$10^5 - 10^6$	$10^6 - 10^7$
Time resolution	100ps	also $< 100ps$
Granularity	$1mm^2$	$1cm^2$
Dynamic Range	limited (Npix)	linear over keV-MeV range

Table 2: Comparison of SiPM to PMT

The determining advantage of SiPM over PMT is their small size, which gives rise to a high granularity and unaffected functionality under magnetic fields, important for the combined use of PET and MRI. A SiPM consists of 3600 APDs that convert electromagnetic radiation into electrons. A reverse bias voltage is applied of around 70V, fully depleting the semiconductor of free electron-hole pairs. An incoming photon will transfer its energy to an electron, which will be accelerated towards the negative voltage. For high enough voltages it will excite other electrons on its way, which again will excite further ones. In this way the photon energy is multiplied by a factor of around 10^5 . This process is also temperature dependent, so the gain of a SiPM varies with operation voltage and temperature. The gain was determined from single photon spectra obtained with a 420nm LED, as in Figure 6. The photons are detected via the photo electric effect, therefore the gain can be measured as the difference between two adjacent p.e. peaks. Performing this measurement for various applied voltages gives the gain as a function of voltage, presented in Figure 7. Background effects such as after-pulsing increase exponentially with applied voltage, therefore a voltage of around 71V was used for the following measurements.

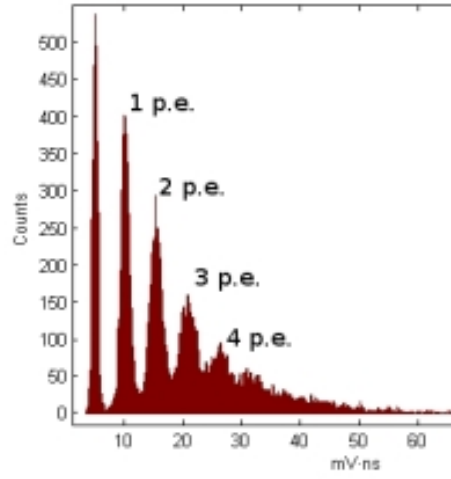


Figure 6: Single photon spectrum for 420nm light. Background pedestal and photo electric multiplicity can be seen.

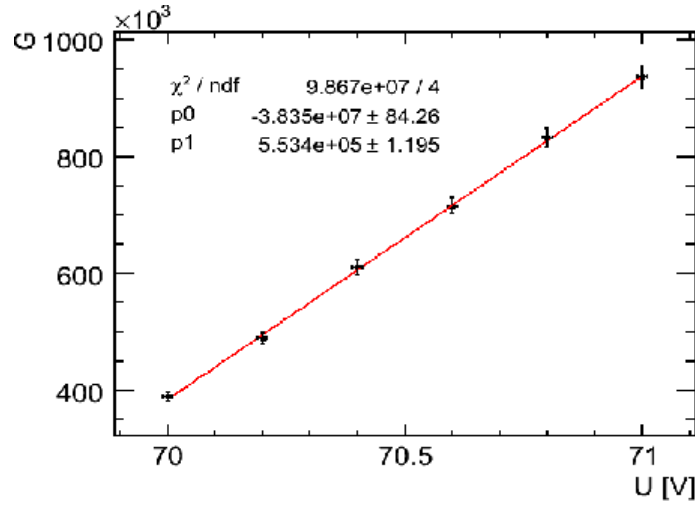


Figure 7: The gain of SiPM is a linear function of the applied voltage.

4 Gamma Ray Spectrum

The cross section of a material depends on its density. Inelastic scattering, in which photons interact with matter, resulting in a change in energy and momentum, is classified as Compton scattering. Compton scattering is described by equation 1, assuming free electrons at rest as scattering objects.

$$E_C = \frac{E_{max}}{1 + \frac{E_{max}}{m_e c^2} (1 - \cos\theta)} \quad (1)$$

Where θ is the scattering angle.

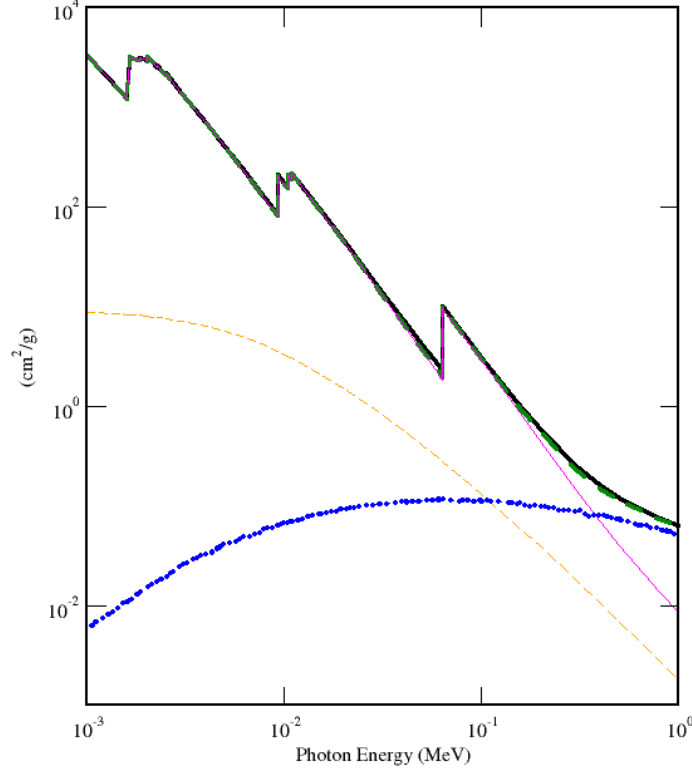


Figure 8: The photo electric cross section(black) of 511 keV is higher than the Compton cross section(blue) in LSO [2].

By not taking the electron momentum into account one introduces an error, which becomes significant for high photon energies, large scattering angles and materials of high Z . For rare events of scattering off protons, the electron mass must be replaced by the proton mass in equation 1.

Large number of photon-matter interactions produce a characteristic spectrum with two contributions. Firstly, a Compton continuum, corresponding to $0 < \theta < \pi$ with a upper limit, the Compton edge. Secondly the photo peak, resulting from photo electric absorption, of magnitude equal to E_{max} . It can be seen from Figure 9 and equation 1 for $\theta = \pi$, that the Compton edge is $2/3$ of the photo peak, clearly separating the two contributions to the spectrum. In reality however, background rate and Gaussian smearing produce energies in this region. The contributions to this smearing are electronic noise and the intrinsic energy resolution of the crystals. These two interaction process have comparable cross sections for LSO crystal, according to Figure 8. A high cross section, especially for photo electric processes is desirable in PET, ensuring maximum detection efficiency. The cross section is inversely proportional to the mean-free-path λ of a photon in matter. The interaction probability I , as in equation 2 is therefore a function of the thickness x of the material and its specific λ .

$$I(x) = I_0 e^{-x/\lambda} \quad (2)$$

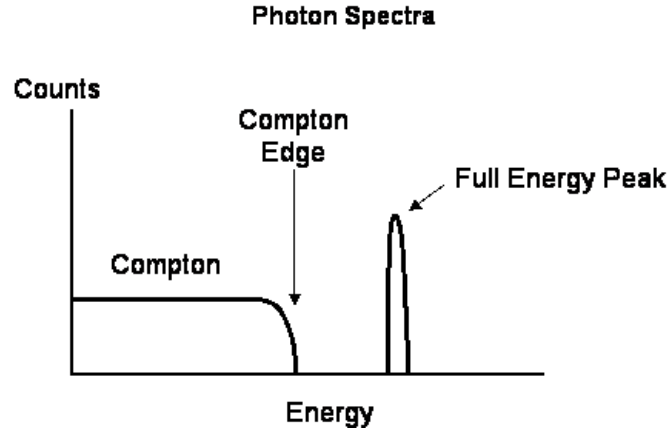


Figure 9: The gamma ray spectrum consists of Compton and photo electric contributions.

5 Motivation - Sensitivity Losses in PET

The sensitivity of a PET device is defined as the proportion of the total emitted photon pairs that produce a coincidence event in two opposing channels, hereby creating a LOR, as in Figure 10a. From equation 2 it can be deduced that a certain fraction of the photons pass the detector without undergoing any interaction.

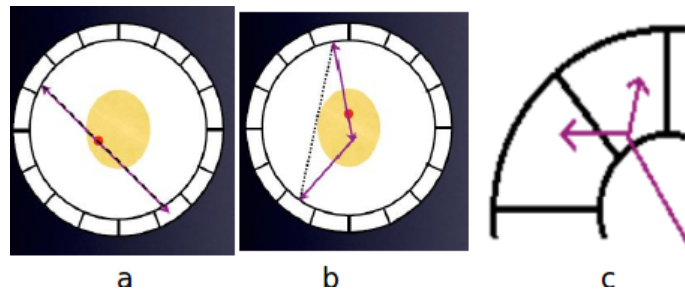


Figure 10: (a) True LOR, (b) False LOR from Compton scattering in the patient, (c) Rejected event due to Compton scattering in the scintillator crystal

Another source of sensitivity loss is Compton scattering in the patient, leading to a false LOR, illustrated in Figure 10b. As such scattered photons will show a decrease in energy compared to unscattered events, given by equation 1, a selection cut at the Compton edge is applied, only taking coincident p.e events into account for PET analysis. A further possibility is that the photons undergo Compton scattering the scintillator material, depositing only a fraction of the p.e peak energy, illustrated in Figure 3c. Such events, although corresponding to a correct LOR, are indistinguishable from scattered coincidences and are therefore rejected by standard PET analysis.

A Monte Carlo simulation Figure 11 shows that for a single 15mm crystal, as used in the prototype, 30% of all 511keV gamma rays incident on the crystal pass through without any interaction and therefore undetected. About 40% deposit 511keV in one p.e (25%)

or in multiple Compton events. Scattering on the surface of the crystal, in the reflective foil or in the metal holder is not taken into account in this simulation. It can be seen from Figure 11 that longer crystals yield greater deposition of all types, however the time resolution degrades by the same amount and for coincidence measurements a good time resolution is critical. The missing 30% that interact in the crystal but do not deposit 511keV are due to Compton scattering where the scattered photon exits the crystal after partial energy deposition.

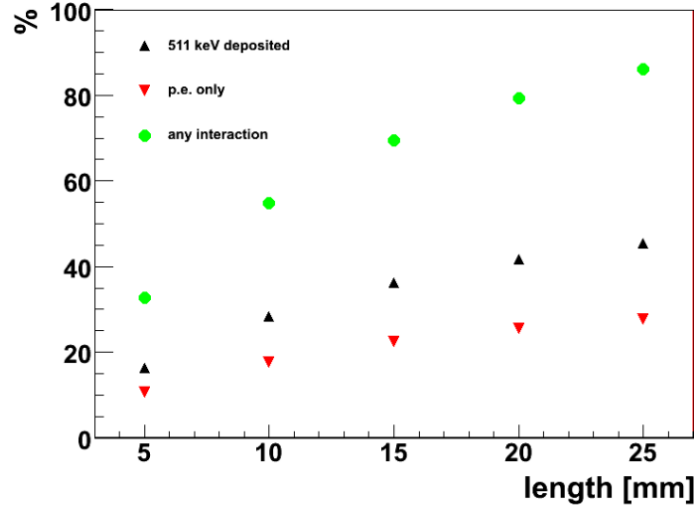


Figure 11: Simulation on single channel efficiency for 511keV gamma rays [4]. Probabilities for any interaction at all, photo electric interaction and 511keV deposition are shown.

A secondary interaction in a neighbouring crystal is highly probable for these cases and summing the energies over two crystals should add to 511keV. Recovering and including such events into the PET analysis would vastly improve the sensitivity. The potential increase in sensitivity and the spatial resolution of such events was investigated in this experiment.

6 Experimental Setup

Although the gain of the SiPM at the used voltage and given temperature was known, the light yield of the crystals and the optical coupling of both components was not. Therefore the energy scaling was obtained by recording spectra of each channel with a Na 22 source, then taking the photo electric to be 511keV. The linearity of the gain was checked by comparing the energy of the photo peak to the energy of the Compton edge, confirming the 2/3 ratio according to equation 1, within 4%. Therefore the Compton edge was taken as the point of maximal slope. As the discrepancy to 2/3 is due to saturation effects, it is to be expected that small energy values are overestimated by maximally 4%. In order to analyse coincident energy deposition in two neighbouring crystals one channel(primary channel) of a 2x2 detector matrix was aligned with a single channel on the

second detector unit, used as a trigger. A Na 22 source was positioned 0.1cm from the primary channel and 5cm from the trigger, as in Figure 12.

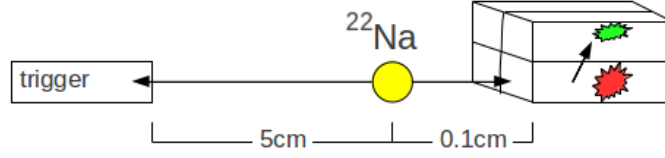


Figure 12: Setup used to investigate Compton scattering in the scintillator crystals.

This geometry prohibits a LOR in the secondary channels, selecting the primary channel as the one with p.e energy deposition. The threshold minimum, sufficient to suppress electronic noise was 50keV. All channels were supplied with an operation voltage of 71V. Data was recorded with the trigger requirements set to

$$E_{trigger} > 50keV \text{ and } (E_{primary} > 50keV \text{ or } E_{anysecondary} > 50keV)$$

Further offline analysis selected events for which

$$400 < E_{trigger} < 600 \text{ and } E_{primary} < 400 \text{ and } E_{anysecondary} \neq 0$$

holds, hereby selecting true LORs where Compton scattering and subsequent energy sharing between two channels occurred.

7 Results

The spectrum obtained for the primary channel showed all the expected characteristics seen in Figure 13 d, with an energy resolution of 11% (σ/μ of photo peak). The overall count is $5.148 \cdot 10^4$ (0-600keV) of which $2.11 \cdot 10^4$ (400-600keV) or 41% fall within the photo peak. This corresponds to a PET sensitivity of 16.8% ($= 41\%^2$) for coincidence detection. The secondary channels, Figure 13 a,b,c show an overall lower count and a smaller photo peak in relation to the Compton continuum than the primary channel.

Energy sharing of two neighbouring channels was confirmed by plotting the primary channel energy against the energy of a secondary, Figure 14a, for all cases where both were non-zero. A clear anti- correlation can be seen. The sum of the primary with any other channel for all where both were non-zero, gives a mean energy of 533keV. The deviation to 511keV is well within the upper limit of an 8% error due to scaling. The energy resolution of these summed events (σ/μ) is 10%, comparable to the photo peak resolution.

The number of recoverable events from summing which fall in the 400-600keV range, obtained from Figure 14b is 4051 or 7.9% of the overall count. The contribution from the secondary channel diagonally across is negligible, where as the secondary channels directly to the left and above contribute in a 3:2 ratio.

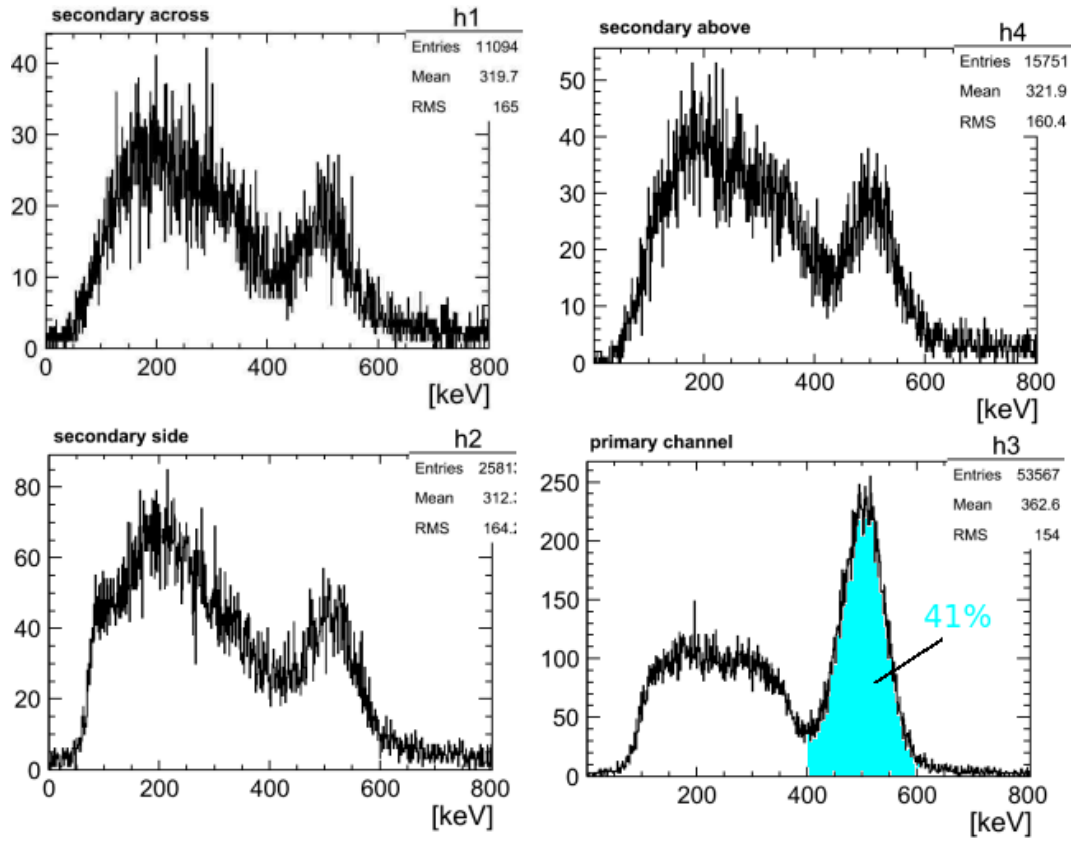


Figure 13: Spectra from all four channels, secondary (a,b,c) and primary (d)

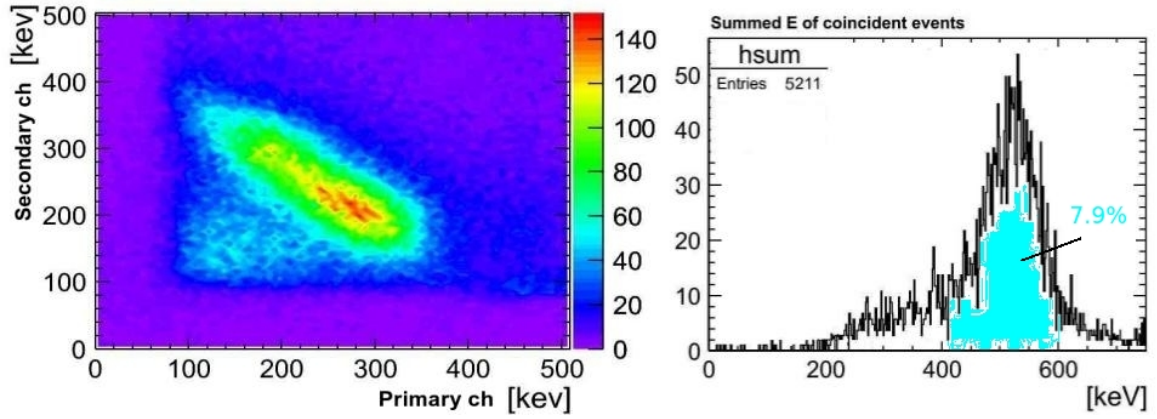


Figure 14: Neighbouring channels experience coincident energy deposition, which is anti-correlated and sums to values equivalent to single photo electric events.

8 Discussion

Applying the obtained result of 7.9% recovery for a 2x2 matrix to 3x3 and larger matrix, as found in real PET arrangements, demonstrates the full potential of this addition to the LOR analysis. In this case, one can assume for large arrays, that in the limit, each channel has four neighbouring ones, from which up to 15.8% recovery can be achieved. An improvement in energy cut from 41% to 56.8% translates to PET sensitivity of 32.3% ($= 56.8\%^2$). Putting this in context to the 16.8% PET sensitivity achieved by standard p.e analysis, this is major increase of about 1.9.

8.1 Reconstruction Issue

For this experiment the true LOR was fixed by the geometry and therefore known. This is not the case in standard PET, where the primary channel must be determined from the pattern of the energy deposition in order to maintain the same spatial resolution as in photo electric events of 2mm. With reference to Figure 8, the cross section, although varies greatly in the keV range, can not be taken as a measure of energy deposition and no prediction can be made if on average more energy is deposited in the primary or secondary channel, due to different total energies. Thus giving no indication to the order in which two channels were hit. This was observed by plotting the weighted position of the channel with deposited energy according to equation 3 as in Figure 15.

$$\bar{x} = \frac{\sum x_i E_i}{\sum E_i} \quad (3)$$

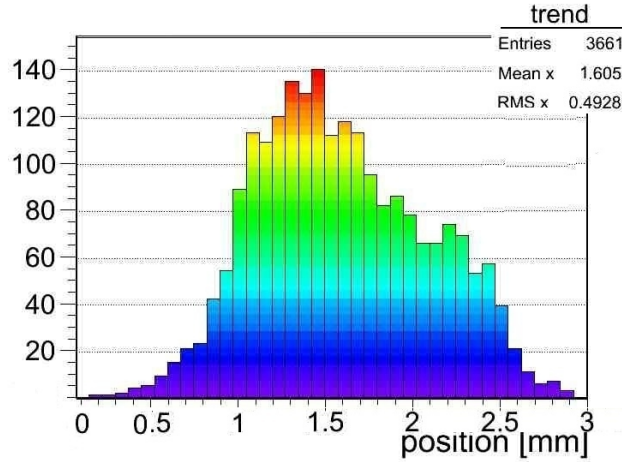


Figure 15: Weighted position by energy. The center of the primary channel is positioned at zero and the center of its nearest neighbour is therefore at 3mm.

It can be seen that no conclusion can be drawn, as the mean of 1.6 compared to the crystal boundary of 1.5 is insignificant to make any prediction. However, it can be expected that a large fraction of the Compton events take place near the crystal border,

in which case recovered events could be assigned to the inter-crystal boundary, partially maintaining the quoted spatial resolution. To validate this assumption a Monte Carlo simulation was constructed, in which the probability of Compton losses was determined for different interaction points in the crystal, shown in Figure 16. It was found that

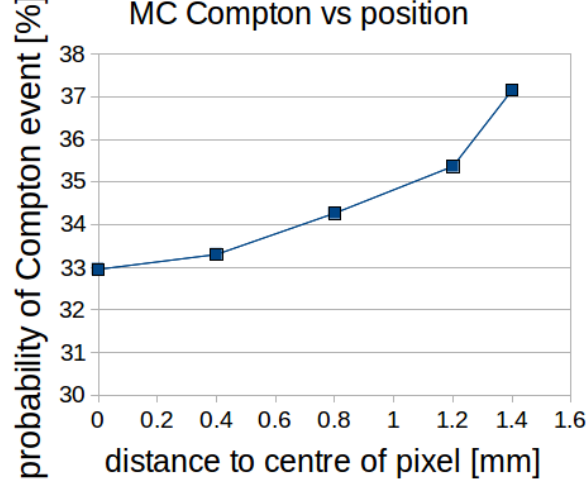


Figure 16: The simulation shows only a small variation in Compton losses as a function of position. The boundary is situated at 1.5mm.

there is only an increase of 11% in the probability of a Compton scattered photon to leave the crystal. This value is insufficient to assign two channel events to the crystal boundary. As a result the uncertainty in position where the gamma ray hit the detector σ_D is increased from 1.5mm (half the crystal width) to 3mm. The minimum spatial resolution σ_R of the PET system is given by the combination of σ_D , the mean free path of the R_{mean} and the non-collinearity of the back to back photons σ_{nc} .

$$\sigma_R = \sqrt{R_{mean}^2 + \sigma_D^2 + \sigma_{nc}^2} \quad (4)$$

with $\sigma_{nc}=0.0044R$, where R is the PET radius. For example, for a human PET of $R=500\text{mm}$ and $R_{mean}=0.6\text{mm}$, Figure 2 for FDG in water, the increase in σ_D causes an increase of 28% in σ_R (2.72mm to 3.78mm) by equation 4.

The fact that the spectra of the secondary channels in Figure 13 show a relatively small photo peak around 511keV is an indication that the geometric selection of the primary channel needs improving. These unexpected LOR can not be explained non-collinearity of the coincident gamma rays. Additionally, the count of the channel diagonally across from the primary, Figure 13a, is far higher than expected. Assuming perfect alignment the detection count should be negligibly small, as the contact surface is infinity small with the primary channel, compared to the other two secondary. Further beam tests are necessary to eliminate these effects and to make a final statement on the energy deposition pattern over two crystals for a known true LOR.

8.2 Readout Issue

In order to recover Compton events in coincidence as described, the signal of up to 10 channels must be readout simultaneously, compared to two for standard analysis. Furthermore the threshold must be reduced from 400keV to about 50keV, resulting in an increase in data rate of 2.5 per channel, or an overall increase in data volume by a factor of 12.5($=5 \times 2.5$). This number is an lower limit estimate, as Compton interactions in the patient's body are present in real PET, thus increasing the Compton count even further. In that case the energy cut would also be far below 40%. A test with the source surrounded by water instead of air would give an indication of how much this increase would be. The analysis in this report was conducted offline, but performing it online, as in real PET imaging, would require additional front-end trigger logics. Such an extension of the readout electronics is a low cost upgrade, with limited size increase to a tomograph.

9 Conclusion

Preliminary evaluation of the SiPM chips was undertaken, determining setting for the actual experiment. Investigation into recovery off Compton events in PET analysis was successfully conducted. It was found that the sensitivity of PET devices can be improved by a maximum factor of 1.9, by taking multichannel energy deposition into account. These additional events have up to twice the spatial resolution for a small PET radius, however further investigation into this is necessary. The capacity of the current data acquisition electronics to deal with an order of magnitude increase in data volume must be evaluated and potentially upgraded, in order to process these additional events. The results obtained are applicable to a low density material ,such as air, surrounding the source. Further research on the effect of Compton scattering in biological tissue on the data rate is needed.

10 Acknowledgements

Special Thanks to Alessandro Silenzi, Chen Xu and Erika Garutti for their help and support during my time at FLC Desy.

References

- [1] Positron Emission Tomography, Present status and future prospects, NDIP 2011 conference www.ndip2011.fr, July 2011 *S. Tavernier*
- [2] www.nist.gov
- [3] Positron Emission Tomography, Springer, 2005 *Dale L. Bailey, David W. Townsend, Peter E. Valk, Michael N. Maisey*
- [4] Single channel aspect optimization, Internal Note, April 2011 *Martin Göttlich*
- [5] Positron Emission Tomography, Springer, 2005
Dale L. Bailey, David W. Townsend, Peter E. Valk, Michael N. Maisey